~~CONFIDENTIAL~~

NASA TM X-630

TECHNICAL MEMORANDUM

X-630

AERODYNAMIC CHARACTERISTICS OF A FLAT-BOTTOM CANTED-NOSE HALF-CONE REENTRY CONFIGURATION AT A MACH NUMBER OF 6.7

By William O. Armstrong

Langley Research Center
Langley Air Force Base, Va.

NATIONAL AERONAUTICS AND SPACE ADMINISTRATION
WASHINGTON
February 1962

~~CONFIDENTIAL~~

NATIONAL AERONAUTICS AND SPACE ADMINISTRATION

TECHNICAL MEMORANDUM X-630

AERODYNAMIC CHARACTERISTICS OF A FLAT-BOTTOM CANTED-NOSE HALF-CONE REENTRY CONFIGURATION AT A MACH NUMBER OF 6.7*

By William O. Armstrong

SUMMARY

An investigation was conducted in the Langley 11-inch hypersonic tunnel to determine the trimmed longitudinal and lateral stability and control characteristics of a flat-bottom half-cone reentry configuration with a blunt canted nose. Data were obtained at a test Mach number of 6.7 and a free-stream Reynolds number per inch of 0.12×10^6. The configuration was studied through an angle-of-attack range from -5° to 77° and at angles of sideslip from -5° up to 10°. Although Newtonian estimates were shown to provide an adequate means for estimating the trends in the longitudinal aerodynamic characteristics of the vehicle, in certain angle-of-attack regions discrepancies between theory and experiment became significant.

The results of this investigation indicate that a canted-nose flat-bottom half-cone configuration can be made longitudinally and laterally stable and controllable through a range of angle of attack from approximately 30° to 75° covering a variation in lift-drag ratio from the maximum to zero. Differential deflection of a split horizontal flap control produced serious roll-yaw coupling when the flap was hinged about a line normal to the body longitudinal axis. Geometric modifications which directed the yaw-producing vector of the roll control surface through the vehicle center of gravity provided an effective means of eliminating this problem. Reduced roll and yaw control effectiveness were experienced at high angles of attack.

INTRODUCTION

Studies are currently under way at the National Aeronautics and Space Administration to investigate configurations suitable for reentry

*[redacted]

from supercircular orbit. While a ballistic trajectory is considered satisfactory for reentry from a circular orbit, studies have indicated that some form of lifting vehicle is expected to be required for reentry from a lunar mission. Numerous results have been published showing the gains in maneuverability, reduction in reentry deceleration and heating rates, and increases in corridor width achieved through use of lift (see refs. 1 to 4). Most of the reduction in reentry deceleration and increase in corridor width occurs in the range of lift-drag ratio below 0.5 (refs. 2 to 4); therefore, for a minimum-weight vehicle current thinking generally favors a design having a maximum lift-drag ratio on the order of 0.5 for return from supercircular orbit.

Numerous shapes have been investigated as possible vehicle designs suitable for return from lunar orbit (for examples, see refs. 5 to 11). The configuration considered herein was evolved from the results of a generalized study of the characteristics of various conic and elliptic body shapes presented in reference 8. Basically this design consists of a flat-bottom half-cone body having a blunt flat canted nose. The flat-bottom configuration was chosen since it was shown in reference 9 to have some advantage in lift, lift-drag ratio, and total heat load over the round-bottom half-cone. It was also pointed out in reference 9 that the flat canted nose provides a useful input to longitudinal trim without significantly altering the lift-drag characteristics of the vehicle. Canted triangular slabs were incorporated in this design as side surfaces to provide greater lateral and directional stability than was achieved by the basic half-cone shape. A short-chord full-span split horizontal flap and canted side fins were used to provide pitch, roll, and yaw control.

Considerable data on this and several other possible reentry shapes are presented in reference 7 for Mach numbers up to approximately 10. Heat-transfer and pressure data on a model similar to this configuration are presented in reference 10. The purpose of this paper is to present a more complete coverage of the longitudinal and lateral stability and control characteristics of the blunted flat-bottom half-cone body at a Mach number of 6.7. Some deficiencies of the initial design are exposed, and the results of tests on several design modifications for alleviating these deficiencies are included. In addition, the ability to predict some of the characteristics of this vehicle by use of modified Newtonian theory (ref. 12) is also assessed.

SYMBOLS

The reference axes systems about which the force and moment coefficients are presented are shown in figure 1. The longitudinal aerodynamic coefficients were referenced to the stability axis system while

the lateral and directional aerodynamic coefficients were determined with reference to the body axis system. Control-surface deflection angles are indicated on figure 2. The various symbols used herein are as follows:

C_A axial-force coefficient, $\frac{\text{Axial force}}{q_\infty S}$

C_D drag coefficient, $\frac{\text{Drag}}{q_\infty S}$

C_L lift coefficient, $\frac{\text{Lift}}{q_\infty S}$

C_l rolling-moment coefficient, $\frac{\text{Rolling moment}}{q_\infty Sc}$

C_m pitching-moment coefficient, $\frac{\text{Pitching moment}}{q_\infty Sc}$

C_N normal-force coefficient, $\frac{\text{Normal force}}{q_\infty S}$

C_n yawing-moment coefficient, $\frac{\text{Yawing moment}}{q_\infty Sc}$

C_p pressure coefficient

C_Y side-force coefficient, $\frac{\text{Side force}}{q_\infty S}$

C_{l_β} rolling-moment derivative, $\frac{\partial C_l}{\partial \beta}$

C_{n_β} yawing-moment derivative, $\frac{\partial C_n}{\partial \beta}$

C_{Y_β}	side-force derivative, $\frac{\partial C_Y}{\partial \beta}$
$C_{l_{\delta a}}$	change in rolling moment with aileron deflection, $\frac{C_l}{\delta_a}$, per deg
$C_{n_{\delta a}}$	change in yawing moment with aileron deflection, $\frac{C_n}{\delta_a}$, per deg
ΔC_m	incremental pitching-moment coefficient, $C_{m,\text{flap on}} - C_{m,\text{flap off}}$
c	moment reference length, 2R (see table I)
L/D	lift-drag ratio
M	Mach number
q	dynamic pressure
R	base radius
r	radius
S	reference area (see table I)
X,Y,Z	body coordinate axes (see fig. 1)
x	coordinate measured along X-axis
x_{cg}	distance to center of gravity along X-axis
z_{cg}	distance to center of gravity along Z-axis
α	angle of attack (see fig. 2), deg
β	angle of sideslip, deg
δ	control deflection angle, deg
δ_a	aileron deflection angle, $\delta_{e,R} - \delta_{e,L}$, deg
η	angle between the velocity vector and a vector normal to the body surface, deg

ϕ angle between body radius and Y-axis, deg

ψ angle measured on the bottom surface between the body center line and a ray passing through the imaginary body apex, deg

Subscripts:

e elevon

L left

max maximum

r rollevator

R right

s side fin

t tab

∞ free-stream conditions

MODELS

Drawings showing the model details of the various configurations tested during this investigation are presented in figure 2. All linear dimensions shown on this figure are nondimensionalized in terms of the body base radius. For the models studied during this investigation, the base radius was 1.635 inches. Photographs of these configurations are shown in figure 3. Although the photographs show considerable indentations in the region of the screws used to attach the flaps, these indentations were filled with plaster before the models were tested. For purposes of conformity, the model designations used in reference 7 were followed in this paper also.

The configuration designated L-1 consisted of essentially a flat-bottom half-cone body having a flat, blunted nose canted 47° from the cone center line or body longitudinal axis. The bottom surface of the body was sloped 7° with respect to the center line or body axis in order to increase the projected side-view area behind the configuration center of gravity and thereby to increase the directional stability of the vehicle. Since canting fins from the vertical has been shown to improve the high-angle-of-attack directional-stability characteristics at hypersonic speeds (ref. 13), slab sides and fins having a 10° cant from the vertical were incorporated in this vehicle. Pitch control was achieved

through use of a short-chord full-span split flap attached to the trailing edge of the bottom surface and having an area equal to 0.1S. Side fins, also having an area equal to 0.1S, hinged at the juncture of the model base and the slab sides, were used to provide directional control. Differential deflections of the split horizontal control flap were used to provide roll control. (See note in fig. 2.)

Configurations which derive roll control through use of a differentially deflected split horizontal flap have been found to encounter significant adverse roll-yaw coupling. (See refs. 14 and 15.[1]) Since roll control for the L-1 model was derived by the same method as that used for the configurations presented in references 14 and 15, roll-yaw coupling might be anticipated for the L-1 configuration also. Since this roll-yaw interaction may possibly stem from a differential axial force on the differentially deflected horizontal flap, a design modification which directs the component of the flap resultant force in the XY-plane through the vehicle center of gravity may offer a means of eliminating the cross-coupling effect. This concept was incorporated into the modifications of the L-1 model investigated and constituted the major difference between the modified models and the initial L-1 design.

The modified configuration designated model L-1B differed from the original L-1 model in that the planform of the pitch flap was trapezoidal in shape (see fig. 2) with triangular outside tips which deflected differentially for roll control. The total flap area remained the same as for the L-1 model (0.1S); however, the area of each of the tip controls was about 1.1 percent of the reference body area (see table I). Roll control of the L-1C configuration was accomplished by means of a roll-evator deflected downward from each rear corner of the bottom surface as shown in figure 2. As noted in table I, the area of each of these control surfaces was about 2.5 percent of the body reference area. Otherwise, the L-1C model was identical to the L-1 model.

The three previously mentioned configurations had the vehicle center of gravity located at a point 0.586R ahead of the base and 0.284R above the body axis (see table I). This center-of-gravity location was selected to provide acceptable longitudinal and lateral stability characteristics and yet still remain in a region of close proximity to that determined by weight and balance estimates of a realistic reentry vehicle (see ref. 7). The projected planform area excluding control-surface area was chosen as the body reference area, and a reference length equal to twice the body radius was used for all data presented. (See table I.)

---

[1]Since only the right half of the flap was deflected, reference 15 does not show this characteristic directly; but the data of reference 15 may be used to compute the case for the differentially deflected elevons from which this adverse yaw can be determined.

For the L-1D configuration, the L-1 model was modified by sweeping the hinge line of the horizontal flap rearward, as shown in figure 2. As a result of this rearward sweep in the flap hinge line, some additional area was added to the rear portion of the bottom surface of the body. (See the L-1D configuration on fig. 2.) The addition of this area to the rear portion of the model required a 2.5 percent rearward shift in the center-of-gravity location used for the three previous models (see table I) in order to maintain high-angle-of-attack trim capability similar to that exhibited by the other models. The flap area remained the same as for the other models. For purposes of comparison, the body reference area and reference length of the three previous models were retained for this configuration also.

APPARATUS AND TEST PROCEDURES

These tests were conducted in the Langley 11-inch hypersonic tunnel at an average Mach number of 6.7 and an average stagnation pressure of 300 in. Hg absolute. The average test free-stream Reynolds number per inch was 0.12×10^6. Stagnation temperature was maintained near 600° F to prevent liquefaction of the air in the tunnel test section. Absolute humidity was kept to a value less than 1.9×10^{-5} pounds of water per pound of dry air. Test data were obtained through an angle-of-attack range from -5° to 77° and an angle-of-sideslip range from -5° to 10°.

The force and moment data presented herein were obtained by means of an internal six-component strain-gage balance mounted through the base of the model. The angles of attack and sideslip of the models were measured optically by means of a lens prism attached to the model base which reflected a point-source light beam onto a calibrated scale. This method allowed the angles of attack and sideslip to be determined irrespective of the deflection of the balance and sting under load.

Base-pressure corrections to the axial force at all angles of attack were made by correcting to free-stream static pressure the measured pressures within the 0.75-inch-diameter balance shield and the assumed pressure coefficient of $-1/M^2$ over the remaining portion of the model base. In no case did this correction exceed 4 percent of the measured axial force, and in most cases the correction was much less than this amount.

ACCURACY OF DATA

The mean-square errors in the force and moment coefficients due to the strain-gage balance system were as follows:

C_L 0.0088
C_D 0.0087
C_m 0.0028
C_l 0.00069
C_n 0.0027
C_Y 0.0028

However, the data were generally found to be more accurate than the values of these errors indicate.

Angle of attack was measured to within $\pm 0.1^\circ$ of the nominal value. Sideslip angle was determined within $\pm 0.1^\circ$ at the lower angles of attack ($\alpha < 50^\circ$) and to an accuracy of $\pm 1.0^\circ$ at angles of attack above 50°. Mach number was determined to within ± 0.05, and stagnation pressure was measured to an accuracy of ± 2.0 in. Hg.

RESULTS AND DISCUSSION

Longitudinal Characteristics of the L-1 Configuration

In order to minimize the heat-protection requirements of the L-1 vehicle, this configuration was designed to operate at relatively high angles of attack where the nonlifting surfaces of the body would be shielded from flow. The longitudinal characteristics of the L-1 model presented in figure 4 show the configuration to be trimmable over an angle-of-attack range from 25° to 75°. The vehicle is found to be stable throughout this entire range of angle of attack and attains a trimmed value of $(L/D)_{max}$ of approximately 0.6 at $\alpha = 30^\circ$ and a trimmed value of $C_{L,max}$ of approximately 0.6 at $\alpha = 42^\circ$. As seen from figure 4, much greater control deflections or an increase in control size would be required to attain trim in the angle-of-attack range below 25°. If trim is desired in this range, additional heat protection would be required for the exposed upper conic surface.

The unusual lift characteristics of this vehicle through the medium angle-of-attack range ($10^\circ < \alpha < 30^\circ$) indicated by the concavity of the lift curve is characteristic of canted-nose configurations of this type, as shown by results presented in reference 8 for models with similar canted noses. The lift characteristics in this angle-of-attack range are also probably largely responsible for the rather small change in the value of lift-drag ratio with α near $(L/D)_{max}$ as indicated by the flat region in the curve for lift-drag ratio (fig. 4). The maximum

drag coefficient of 1.6 occurs at a value of $C_{L,trim}$ of 0.22 ($\alpha = 68^\circ$) and is very nearly the maximum resultant force coefficient attained by the vehicle.

Comparison of Predicted and Experimental Characteristics of the L-1 Configuration

Longitudinal aerodynamic characteristics.- In an effort to assess the ability to predict the basic longitudinal aerodynamic characteristics of the L-1 vehicle by using modified Newtonian theory $\left(C_p = C_{p,max} \cos^2\eta\right)$, a comparison was made in figure 5 between experimental data and theoretical predictions for the basic L-1 body. Although Newtonian theory is shown to provide an adequate means for estimating the trends in the longitudinal aerodynamic characteristics of the vehicle, examination of this figure indicates that in certain angle-of-attack regions discrepancies between theory and experimental results become significant. Both C_L and C_D are underpredicted in the low angle-of-attack range ($\alpha < 10^\circ$). As previously mentioned, experimental values of C_L show a region of concavity in the α range from 10° to 30° which is not indicated by theory. The predicted value of $C_{L,max}$ is shown to be about 6 percent lower than that attained experimentally, although the angle of attack for $C_{L,max}$ is correctly predicted. It is only at the high angles of attack where the body normal-force contribution to lift is unimportant and the body axial force is small that good agreement between theoretical and experimental values of C_L were achieved. However, predicted values of C_D fall well above experimental results in this high angle-of-attack region.

Since theory is unable to predict the detailed lift and drag characteristics of the vehicle, the relatively poor agreement for angles of attack below 45° between theoretical and experimental values of L/D shown in figure 5 would be anticipated. The fact that theory does reasonably approximate the value of $(L/D)_{max}$ is, of course, fortuitous since both lift and drag are inadequately predicted in the angle-of-attack range near $(L/D)_{max}$.

Pitching-moment coefficient is somewhat overpredicted throughout the entire angle-of-attack range, but theory does provide a fairly good estimate of the longitudinal stability of the vehicle. Both theory and experiment show an unstable region at low angles of attack ($\alpha < 20^\circ$), and both show the vehicle to be stable for angles of attack above 30°.

In order to explain the inadequacy of Newtonian theory in predicting the longitudinal characteristics of [redacted] figuration, an examination

of the local pressure distribution over the various surfaces is desirable. Unpublished preliminary pressure distributions obtained in the Langley 20-inch Mach 6 tunnel on the L-1 model at low angles of attack ($\alpha < 10^\circ$) indicate that the pressure distribution over the canted nose is considerably underpredicted by theory. This underprediction of the nose pressure would account for the low estimated values of both C_L and C_D in the low angle-of-attack range previously mentioned.

Pressure distributions at higher angles of attack for the L-1 type of configuration at $M = 9.6$, some of which are published in reference 10, are presented in figure 6. These results, which are substantiated by unpublished test results in the Langley 20-inch Mach 6 tunnel, show that at $\alpha = 15^\circ$ experimental pressures were higher than predictions on the upper section of the nose; however, the area affected was relatively small. Over most of the nose area Newtonian estimates of the pressure coefficient were higher than those obtained experimentally, so that the predicted net integrated force on the nose would be expected to be higher than the experimental. Pressures on the conic and bottom surfaces, on the other hand, are somewhat underpredicted on the forward section at $\alpha = 15^\circ$ (see fig. 6) where carryover effects from the nose section influence pressures on the forward portion of the conic and bottom surface. However, these predictions tend to come into fair agreement with the experimental pressures toward the rear of the model for both surfaces.

Analysis of these pressure data indicate that Newtonian theory does not correctly predict pressures behind large detached shocks generated by blunt bodies of this type and suggests that the overprediction of C_L and C_m in the angle-of-attack range from 10° to 30° results from overprediction of the force on the canted nose. Even though the cone and bottom-surface pressures are underpredicted, lift and pitching-moment contributions of these surfaces are cancelling. However, somewhat better predictions were obtained for C_D in this α range because the drag contributions of the cone and bottom surface are additive, so that the underestimation of the pressures on these surfaces tends to offset the overprediction of the pressures on the nose.

It should be mentioned that while neither the configuration nor the Mach number for the results presented in figure 6 was the same as for the results presented herein (see ref. 10), these data should still be applicable for the purpose intended, since results presented in references 8 and 9 show that configurations of the L-1 type exhibit similar aerodynamic characteristics. The concavity of the lift curve and the unstable pitching-moment curve slope at low angles of attack ($\alpha < 30^\circ$) are characteristic of this class of configuration. It has also been indicated that Mach number effects are of secondary importance for

relatively blunt models of this type in the hypersonic speed range. (See refs. 7 and 9.)

As angle of attack is further increased to that near $C_{L,max}$ ($\alpha \approx 45^\circ$), results presented in figure 6 show the pressures on the entire nose to be overpredicted by theory, while those on the bottom surface are underpredicted. The conic surface is essentially shielded at this angle of attack and makes no significant contribution to the longitudinal characteristics of the vehicle. Since the nose is nearly normal to the flow at this value of α (see fig. 2), it has little influence on the lift of the configuration, and the underestimation of C_L is primarily due to the underpredictions by theory of the pressure on the bottom surface. On the other hand, the lower predicted drag contribution of the bottom is more than offset by the excessive predicted drag of the nose and results in a somewhat higher estimated drag coefficient than that obtained experimentally.

At the highest angles of attack considered for this vehicle ($\alpha > 60^\circ$) large pressure bleed-off would be expected to occur near the edges of the vehicle and would reduce the body drag coefficient in this region below that predicted by Newtonian theory.

Lateral and directional stability characteristics.- Since the lateral and directional aerodynamic characteristics of these vehicles were found to be linear through the range of sideslip of the tests ($-5^\circ \leq \beta \leq 10^\circ$), these characteristics are presented in the form of lateral and directional stability derivatives only. Figure 7 presents the experimental lateral and directional stability derivatives of the basic L-1 configuration and the longitudinally trimmed L-1 vehicle equipped with the side fins for vertical control (see fig. 2). Theoretical predictions for the basic vehicle are also included on this figure.

Experimental results show the basic vehicle to be directionally stable throughout the angle-of-attack range. Furthermore, the vehicle exhibits little change in directional stability with change in angle of attack. The trimmed configuration with the added side fins shows essentially the same characteristics as the basic body but, as expected, possesses a slightly greater margin of directional stability.

Both the basic body and the trimmed vehicle show slightly negative effective dihedral at the low angles of attack ($\alpha < 20^\circ$); however, in the range of α from $(L/D)_{max}$ ($\alpha \approx 30^\circ$) to $L/D = 0$ ($\alpha \approx 75^\circ$) the model exhibits a positive effective dihedral which remains essentially constant for values of angle of attack greater than 45°. Although the addition of the side fins and pitch control surfaces somewhat increases the positive effective dihedral characteristics of the vehicle at the

lower angles of attack ($0^\circ < \alpha < 50^\circ$), the opposite is true in the higher angle-of-attack range.

Comparison of the experimental directional stability characteristics of the basic configuration with the results predicted by modified Newtonian theory indicates that although theory somewhat underpredicts the experimental results it does provide an indication of the trends for C_{Y_β} and C_{n_β}. The dihedral effect indicated by the experimental data is not predicted by theory, since Newtonian predictions indicate the vehicle to have a very small degree of positive effective dihedral which reduces to essentially zero at $\alpha = 0^\circ$. The tendency toward increasing positive dihedral with increasing α, as shown by experimental results, is characteristic of results previously observed on delta-wing configurations (see ref. 13) and probably results from an increased pressure buildup on the windward portion of the bottom surface for a given sideslip as angle of attack is increased.

Flap effectiveness.- In an effort to assess the capability of Newtonian theory for predicting the control effectiveness of the full-span split horizontal flap used on the L-1 vehicle for pitch control, comparisons between experiment and theory were made for three rather distinct cases of flap deflection:

(1) $\delta_e = 40^\circ$, where the flap was deflected downward below the bottom surface of the body.

(2) $\delta_e = 0^\circ$, where the flap simply formed an extension to the body undersurface.

(3) $\delta_e = -50^\circ$, where the flap was deflected upward away from the bottom surface into a region of expanded flow.

Both theoretical and experimental data for these three cases are presented in figure 8 for an angle-of-attack range extending on either side of the point of trim for each flap deflection. For the case where $\delta_e = 40^\circ$, experimental results show the flap to be far less effective than predicted by Newtonian theory. Schlieren photographs of the L-1 model with this flap deflection, presented in figure 9, show a distinct region of separated flow extending well forward of the flap over the rear portion of the body. This separation obviously must cause a reduction in the pressure over the flap, which accounts for the overprediction of flap effectiveness shown on figure 8.

Good agreement was shown between experimental and predicted results (fig. 8) for the case of the undeflected flap ($\delta_e = 0^\circ$). Schlieren photographs of this case (fig. 9) indicate smooth undisturbed flow over the

entire bottom surface of the body and flap. If the results presented in figure 6 are recalled, which showed good agreement between experimental and predicted pressure distribution over the aft region of bottom surface, good agreement would be expected between experiment and theory for the flap deflection of 0°.

When the flap was deflected upward away from the bottom surface ($\delta_e = -50^\circ$), the flap was found to produce larger nose-down moments than those predicted by theory. This effect also continued to much lower angles of attack than indicated by the theory, which assumes no force on the flap when it is hidden from flow. In this case the flap was located in a region of expanding flow and reducing pressures aft of the bottom surface, as indicated by the darkened regions under the flap shown on the schlieren photograph of figure 9. This situation is similar to the case at the juncture of the nose and bottom surface, where large carryover effects were previously observed (fig. 6) to increase the pressure. Similar carryover effects are obviously present on the flap when it is deflected upward away from the bottom surface, and these effects explain the differences between the measured and predicted results.

Yaw Control of the L-1 Configuration

The effects of the deflected side fins on the lateral and pitch characteristics of the L-1 configuration are presented in figure 10. The side fins were shown to provide relatively little directional control for deflections less than -15°; however, substantial control effectiveness was achieved when the side fins were deflected -45°. The low effectiveness of the side fins for small deflections is largely due to the fact that the fin does not become exposed to flow for $\delta_s < 10^\circ$. (See fig. 2.) Negligible roll-yaw and pitch-yaw coupling is noted for the fin deflections shown on figure 10 up to an angle of attack of 60°. At the higher angles of attack ($\alpha > 60^\circ$), some roll-yaw interaction is evident, but as seen from figure 10, the ratio of yawing coefficient to rolling coefficient is still relatively large but favorable. It should be noted that although yaw control effectiveness is reduced at the higher angles of attack, some control is still available so that side fins should be feasible for aerodynamic yaw control in the hypersonic flow range.

Roll Control of the L-1 Configuration

As previously stated, roll control for the L-1 vehicle was obtained by differentially deflecting the horizontal flap. Results of tests on this model with the differentially deflected horizontal flap are presented in figure 11. Although data were obtained through an angle-of-attack range from 25° to 58° only, figure 11 shows serious roll-yaw

interaction due to the differential deflection of the flap. This adverse yaw due to roll control possibly resulted from the difference in axial force acting on the differentially deflected split horizontal flap.

Because of this undesirable cross-coupling effect, some means was sought to modify the basic L-1 vehicle in an effort to minimize this unsatisfactory characteristic.

If this adverse roll-yaw coupling resulted from a difference in the axial force acting on the differentially deflected split horizontal flap, then canting the hinge line of the horizontal flap rearward so as to direct the component of the resultant force vector in the XY-plane of the flap through or near the vehicle center of gravity offered a readily apparent means of reducing this control interaction. This scheme was incorporated into the L-1D vehicle design (see fig. 2), examined theoretically, and compared with the Newtonian calculations for the configuration with the unswept hinge line (the L-1 configuration). The results of this Newtonian comparison are presented in figure 12. From this figure it can be seen that the rearward canted hinge line greatly reduced the roll-yaw interaction on the L-1D model without seriously affecting the roll effectiveness of the flap. Experimental data also presented on this figure verify the theoretical estimates.

L 1 8 3 1

Roll Control of the L-1D Configuration

Since the adverse roll-yaw coupling was substantially reduced by the L-1D modification (fig. 12), the effect of differential horizontal-flap deflections on the lateral aerodynamic and pitch characteristics of the L-1D configuration were investigated over the entire angle-of-attack range for several flap deflections. The results of these tests are presented in figure 13. Roll control is shown to be quite good for values of α less than 60°. In the high angle-of-attack range roll effectiveness is substantially reduced, and flight-simulation studies would probably be required to determine whether sufficient roll output is available in this range of angle of attack for satisfactory vehicle control. It should be noted, however, that yaw-due-to-roll-control and pitch-due-to-roll-control interactions are quite small over the entire angle-of-attack regime and should pose no problem area in vehicle control.

Longitudinal and Lateral Aerodynamic Characteristics of the L-1D Configuration

The experimental trimmed longitudinal aerodynamic characteristics of the L-1D model are presented in figure 14. It can be seen by comparing

the results presented in this figure with those of figure 4 that the longitudinal characteristics of this configuration are essentially the same as for the L-1 vehicle. The L-1D configuration is stable and trimmable from $(L/D)_{max}$ ($\alpha \approx 25^{\circ}$) to $L/D = 0$ ($\alpha \approx 75^{\circ}$). The model attained a trimmed value of both $(L/D)_{max}$ and $C_{L,max}$ of approximately 0.66. It should be noted that the added area to the bottom surface obtained by sweeping the flap hinge line rearward (fig. 2) required a 2.5-percent rearward shift in the vehicle center of gravity (see table I) in order to maintain stable trim characteristics through the desired α range.

The trimmed lateral stability characteristics for the L-1D model are essentially unchanged from that of the L-1 model, as seen by comparing the lateral stability data of the L-1D model (fig. 15) with similar data for the L-1 model (fig. 7). The slightly lowered values of C_{n_β} and C_{Y_β} for the L-1D model result from the more rearward center-of-gravity location for this model rather than from any change in the flow conditions on the model.

Yaw Control for the L-1D Configuration

Yaw control characteristics for the L-1D model are presented in figure 16. The results presented in this figure agree very closely with those presented in figure 10 for the L-1 model. Adequate control appears to be available throughout the angle-of-attack range considered, although control effectiveness is substantially reduced at the higher angles of attack ($\alpha > 60^{\circ}$) from that obtained at the lower angles of attack. Further, it should be noted that yaw control produces little or no cross coupling in pitch or roll.

Roll Control for the L-1B and L-1C Configurations

Although adverse yaw was substantially reduced for the L-1D model, as previously mentioned the roll control effectiveness of this model was considerably reduced at the higher angles of attack. Two other modifications were also investigated to determine whether better aerodynamic characteristics could be obtained by different roll control configuration. These modifications, designated the L-1B and L-1C models and shown in figure 2, have been previously described in the section entitled "Models." Since these models were almost identical to the L-1 model except for the manner of achieving roll control, the stability and control characteristics (other than roll control) presented previously for the L-1 model would be characteristic of these configurations also. For this reason, data for roll control only are presented for these two configurations.

Roll control characteristics for the L-1B model are presented in figure 17. Although adequate roll control appears to be available up to moderate angles of attack ($\alpha < 60^\circ$), this configuration also showed a marked reduction in roll control in the high angle-of-attack range ($\alpha > 60^\circ$). Although no serious cross-coupling effects were observed, this configuration exhibits no distinct advantage over the L-1D model which would merit its use in preference to that model.

Roll control for the L-1C configuration is presented in figure 18. This figure shows that the L-1C model retained roll control to much higher angles of attack than did the other models; therefore, roll control may be available over the entire angle-of-attack range for the L-1C configuration. Data presented in figure 18 further indicate no significant problem in adverse yaw or pitch coupling with roll. Thus, from the standpoint of stability and control this roll control configuration appears to have satisfactory hypersonic characteristics for use as a reentry vehicle. However, serious structural problems may arise in the design of this vehicle, particularly in the region of the roll control surface, where serious local heating problems may be encountered when the rollevators are deflected.

Longitudinal Trim Characteristics of the L-1 Series Configurations

Figure 19 shows a summary of the longitudinal trim characteristics of the L-1 series models investigated. As previously mentioned, the L-1, L-1B, and L-1C configurations were nearly identical except for the method for obtaining roll control and, therefore, have the same longitudinal trim characteristics. Examination of figure 19 shows that effective trim control was provided for all the L-1 series models over the angle-of-attack range from $(L/D)_{max}$ ($\alpha \approx 25^\circ$) to $L/D = 0$ ($\alpha \approx 75^\circ$) through use of a short-chord trailing-edge horizontal flap capable of flap deflections from 40° to -50°. Only small differences are noted in the flap deflections required for trim for the various vehicles tested.

The L-1D model attains approximately 5 percent more trimmed $(L/D)_{max}$ and 13 percent more trimmed $C_{L,max}$ than the other vehicles, although the angle of attack at which these quantities occurred remained essentially unchanged. The increase in $C_{L,max}$ for the L-1D model was largely due to the added lift of the enlarged bottom surface when the coefficient was based on the same reference area as the L-1 model. As shown in table I, the reference area was held constant, for purposes of comparison, on all the configurations tested.

It should be noted (fig. 19) that trimmed values of L/D from 0 to values approaching 0.5 can be obtained on all these models by using

upward flap deflections only. Thus, these vehicles can attain values of trimmed L/D approaching that required for the lunar mission without resorting to a positive flap deflection. This capability should offer considerable advantage from the standpoint of control-surface heating.

CONCLUDING REMARKS

It has been shown that a canted-nose flat-bottom half-cone configuration can be made longitudinally, directionally, and laterally stable and controllable through an angle-of-attack range from approximately 30° to 75° covering a variation in lift-drag ratio from the maximum to 0. Although Newtonian theory was shown to provide an adequate means for estimating the trends in the longitudinal aerodynamic characteristics of this vehicle, in certain angle-of-attack regions discrepancies between theory and experiment became significant.

Excessive roll-yaw coupling was encountered on the initial design, which derived roll control by means of differential deflections of the split horizontal flap when the flap was hinged about a line normal to the body axis. Geometric modifications which directed the yaw-producing vector of the roll control surface through the vehicle center of gravity essentially eliminated this problem without noticeably affecting the other characteristics of the vehicle.

Both roll and yaw control effectiveness were reduced at the higher angles of attack (greater than 60°). Simulator studies may be required to determine whether these control forces are adequate for satisfactory control.

Langley Research Center,
National Aeronautics and Space Administration,
Langley Air Force Base, Va., December 4, 1961.

REFERENCES

1. Becker, John V.: Re-Entry From Space. Scientific American, vol. 204, no. 1, Jan. 1961, pp. 49-57.

2. Lees, Lester, Hartwig, Fredric W., and Cohen, Clarence B.: Use of Aerodynamic Lift During Entry Into the Earth's Atmosphere. ARS Jour., vol. 29, no. 9, Sept. 1959, pp. 633-641.

3. Grant, Frederick C.: Importance of the Variation of Drag With Lift in Minimization of Satellite Entry Acceleration. NASA TN D-120, 1959.

4. Chapman, Dean R.: An Analysis of the Corridor and Guidance Requirements for Supercircular Entry Into Planetary Atmospheres. NASA TR R-55, 1960.

5. Sarabia, Michael F.: Aerodynamic Characteristics of a Blunt Half-Cone Entry Configuration at Mach Numbers From 3 to 6. NASA TM X-393, 1960.

6. Armstrong, William O.: Effect of Various Forebody Modifications on the Static Longitudinal Stability and Control Characteristics of a Reentry Capsule at a Mach Number of 9.6. NASA TM X-469, 1961.

7. Rainey, Robert, W., compiler: Summary of Aerodynamic Characteristics of Low-Lift-Drag-Ratio Reentry Vehicles From Subsonic to Hypersonic Speeds. NASA TM X-588, 1961.

8. Armstrong, William O.: Hypersonic Aerodynamic Characteristics of Several Series of Lifting Bodies Applicable to Reentry Vehicle Design. NASA TM X-536, 1961.

9. Armstrong, William O., Stainback, P. Calvin, and McLellan, Charles H.: The Aerodynamic-Force and Heat-Transfer Characteristics of Lifting Reentry Bodies. NASA TM X-352, 1960.

10. Coe, Frank S., III, and Feller, William V.: Experimental Investigation of the Pressures, Heat Transfer, and Surface Flow Patterns Around a Blunt Half-Cone Lifting Reentry Body at a Mach Number of 9.6. NASA TM X-589, 1961.

11. Davy, William C., and Seiff, Alvin: A Study of the Stability and Performance of Some Unsymmetrical Truncated Conical Configurations for Lifting Re-Entry. NASA TM X-504, 1961.

12. Penland, Jim A.: Aerodynamic Characteristics of a Circular Cylinder at Mach Number 6.86 and Angles of Attack up to 90°. NACA TN 3861, 1957. (Supersedes NACA RM L54A14.)

13. Ladson, Charles L.: Directional and Lateral Stability Characteristics of a Winged Reentry Vehicle at Hypersonic Speeds. NASA TM X-550, 1961.

14. Ladson, Charles L., and Johnston, Patrick J.: Aerodynamic Characteristics of Two Winged Reentry Vehicles at Supersonic and Hypersonic Speeds. NASA TM X-346, 1961.

15. Clark E. L., and Mallard, S. R.: Force Tests of the AD-540I-1 Dyna-Soar Models at Mach Number 8. AEDC-TN-61-48 (Contract No. AF 40(600)-800 S/A 11(60-110)), Arnold Eng. Dev. Center, Apr. 1961.

TABLE I.- CONFIGURATION CONSTANTS

Configuration	$\frac{S}{R^2}$	$\frac{x_{cg}}{R}$	$\frac{z_{cg}}{R}$	$\frac{c}{R}$	$\frac{\text{Pitch control area}}{S}$	$\frac{\text{Roll control area}}{S}$		$\frac{\text{Yaw control area}}{S}$	
						Right surface	Left surface	Right surface	Left surface
L-1	2.26	0.586	0.284	2	0.1	0.05	0.05	0.05	0.05
L-1B	2.26	.586	.284	2	.1	.011	.011	.05	.05
L-1C	2.26	.586	.284	2	.1	.025	.025	.05	.05
L-1D	2.26	.536	.284	2	.1	.05	.05	.05	.05

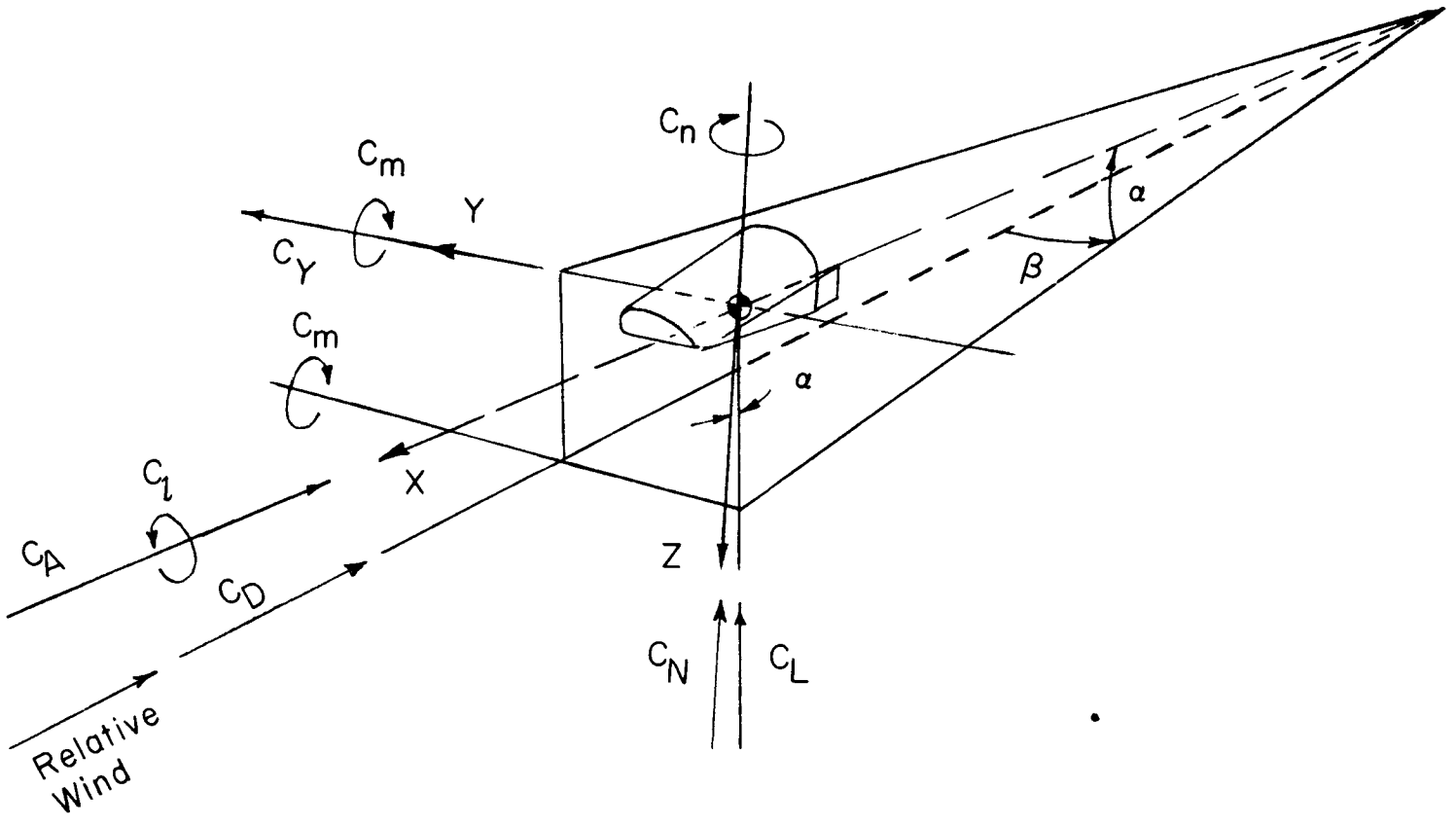

Figure 1.- Axis system with positive directions of forces, moments, and angles indicated by arrows.

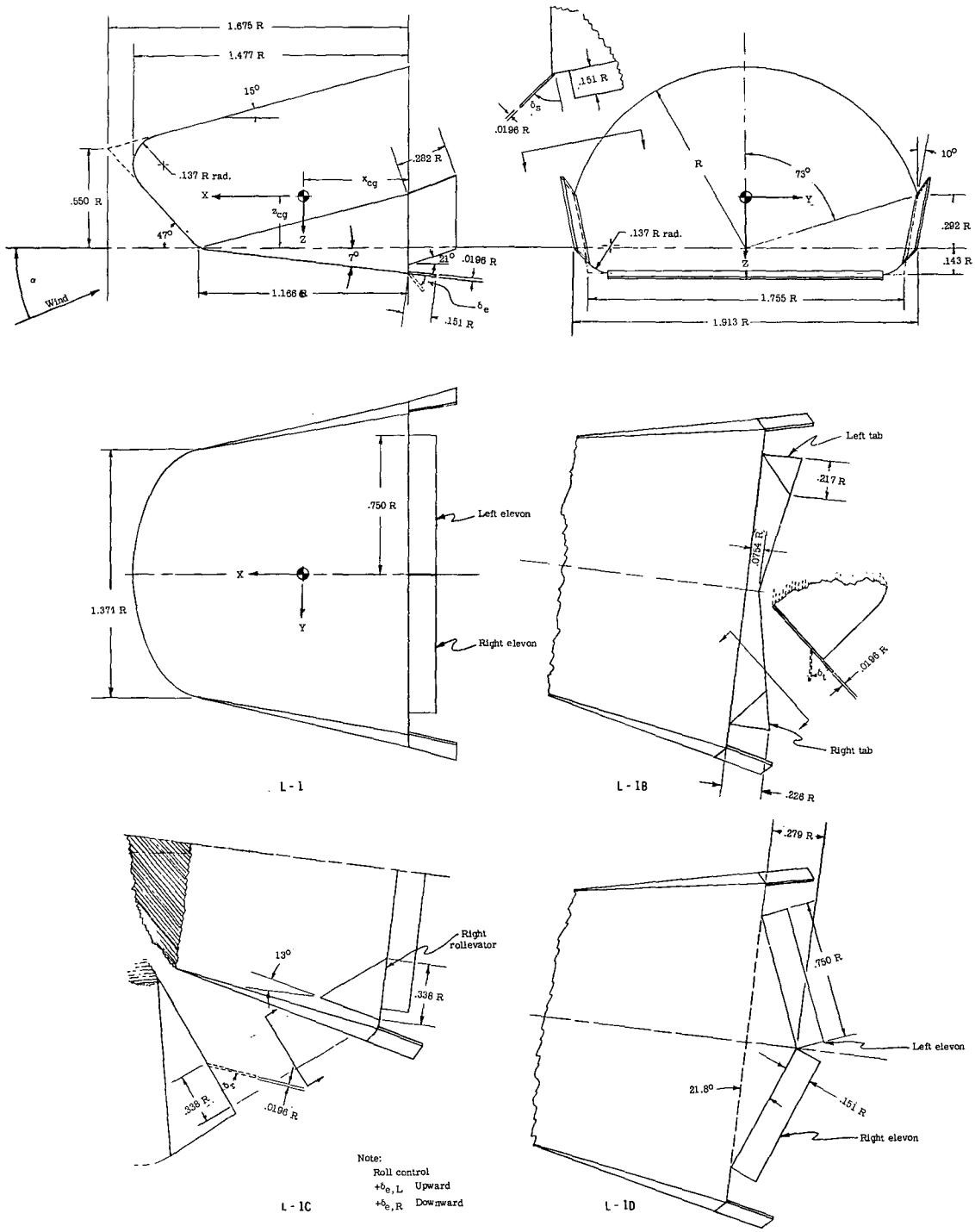

Figure 2.- Sketches of configurations tested.

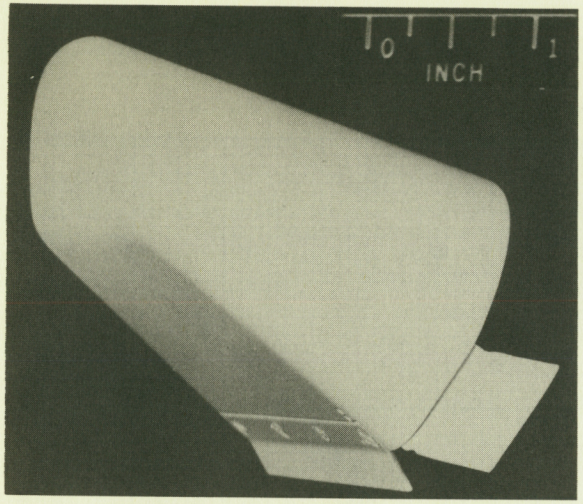

L-1

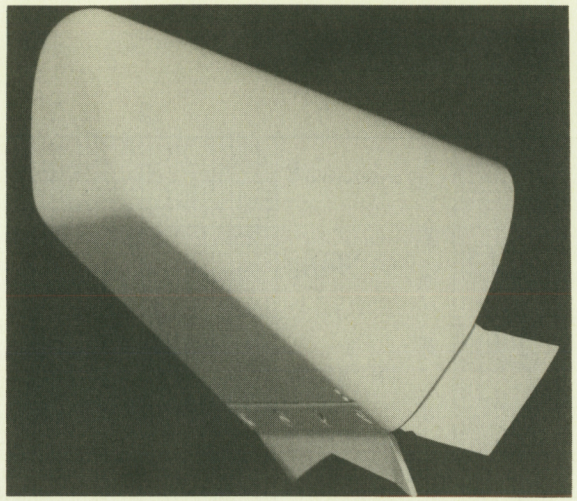

L-1B

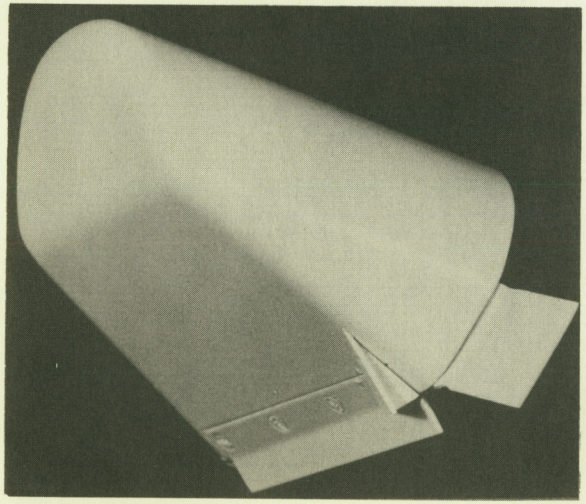

L-1C

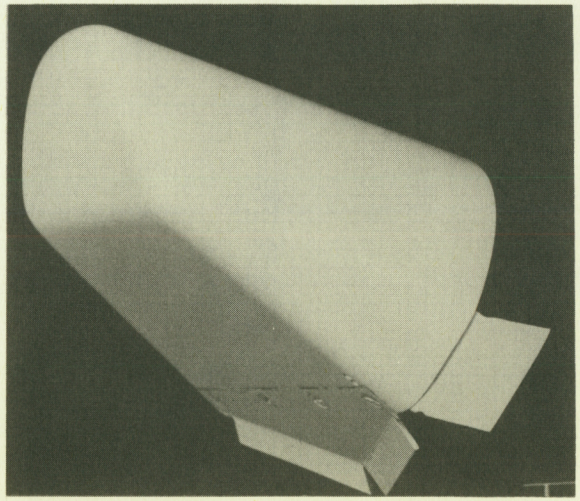

L-1D

Figure 3.- Model photographs. L-61-8051

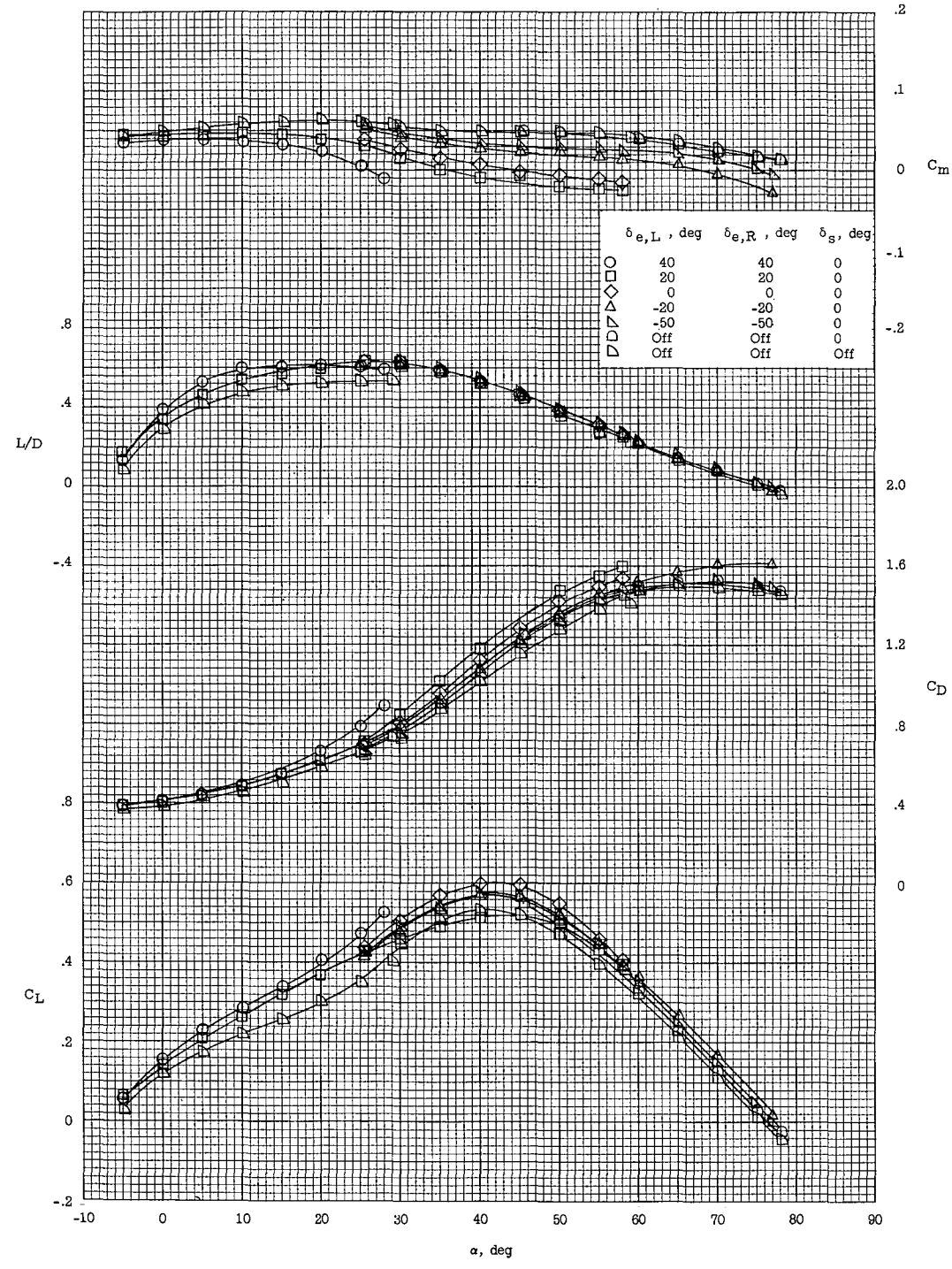

Figure 4.- Experimental longitudinal aerodynamic characteristics of the L-1 configuration.

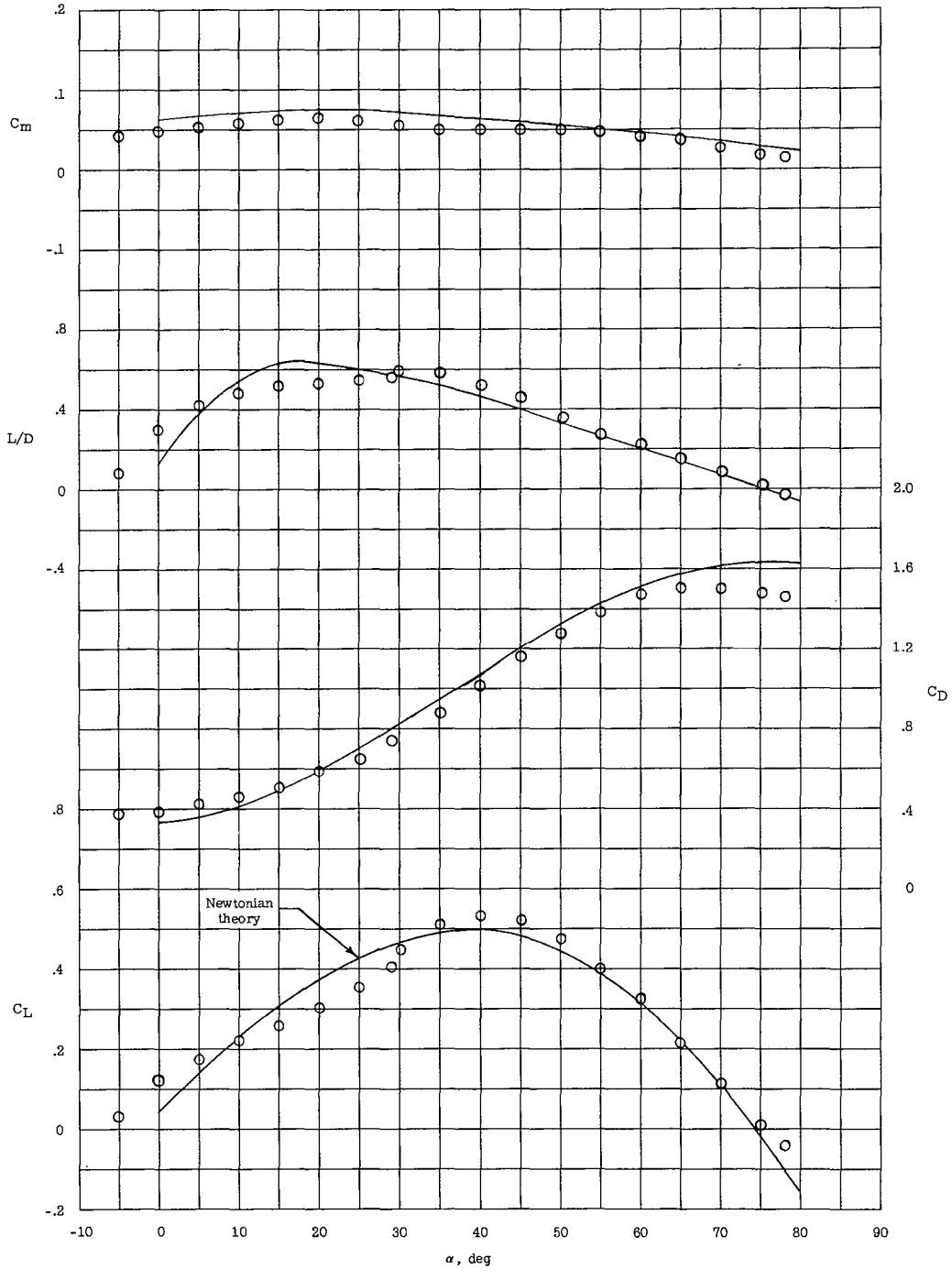

Figure 5.- Comparison of the predicted and experimental longitudinal aerodynamic characteristics of the L-1 basic configuration (no flaps or vertical fins).

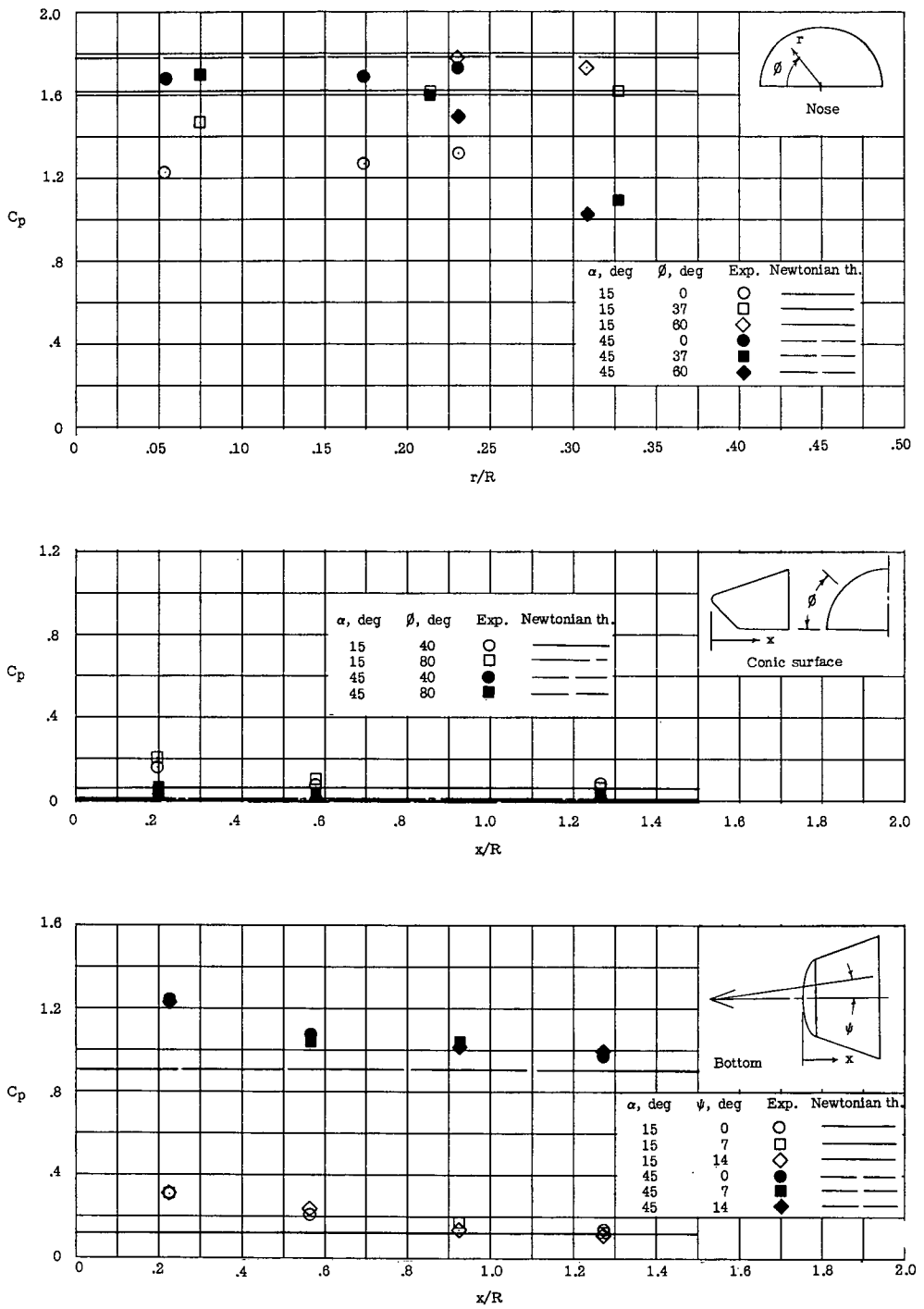

Figure 6.- Comparison of predicted and experimental pressure distribution on the L-1 type of configuration of reference 10 at M = 9.6.

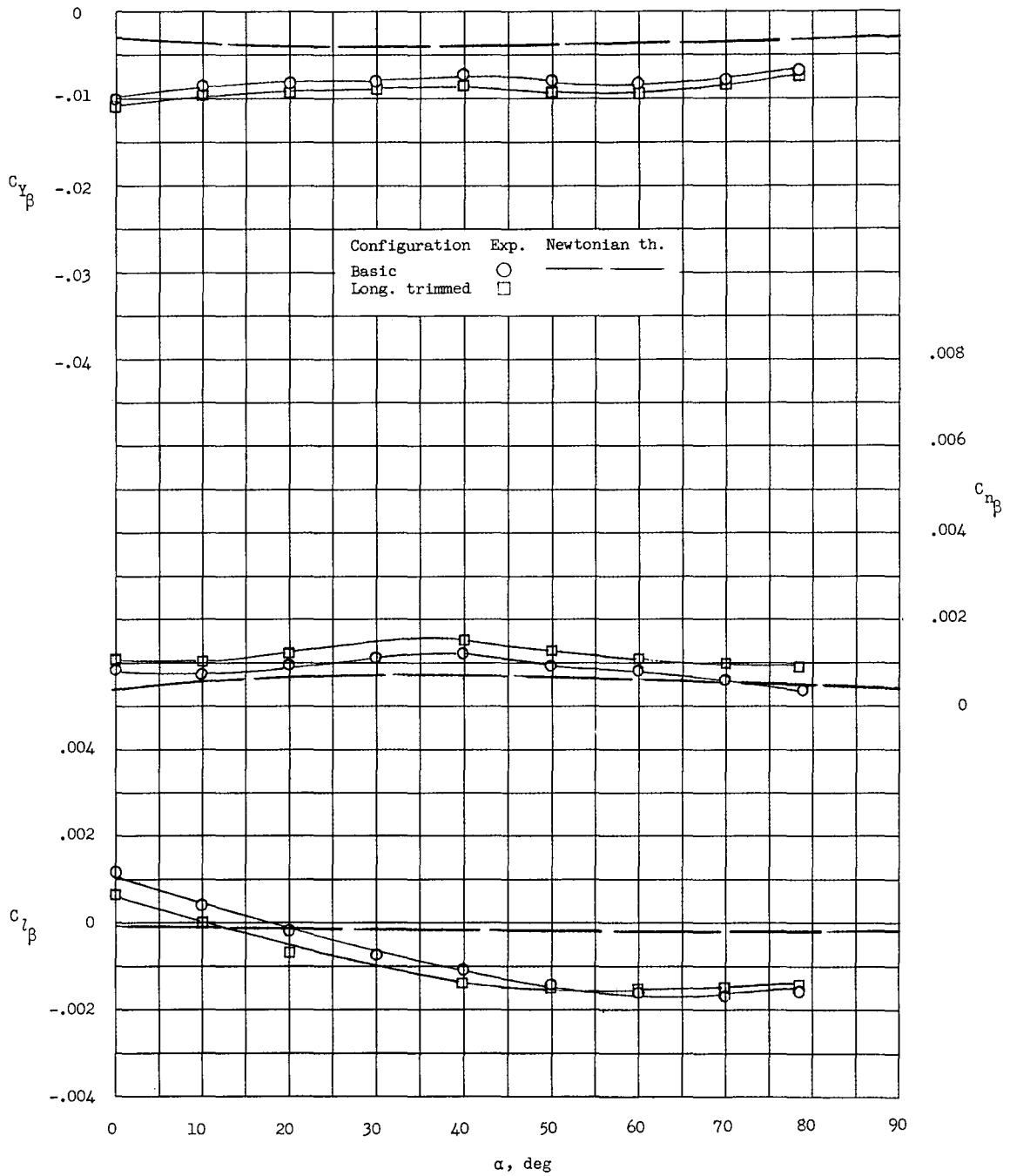

Figure 7.- Comparison of the predicted and experimental lateral stability characteristics of the L-1 configuration.

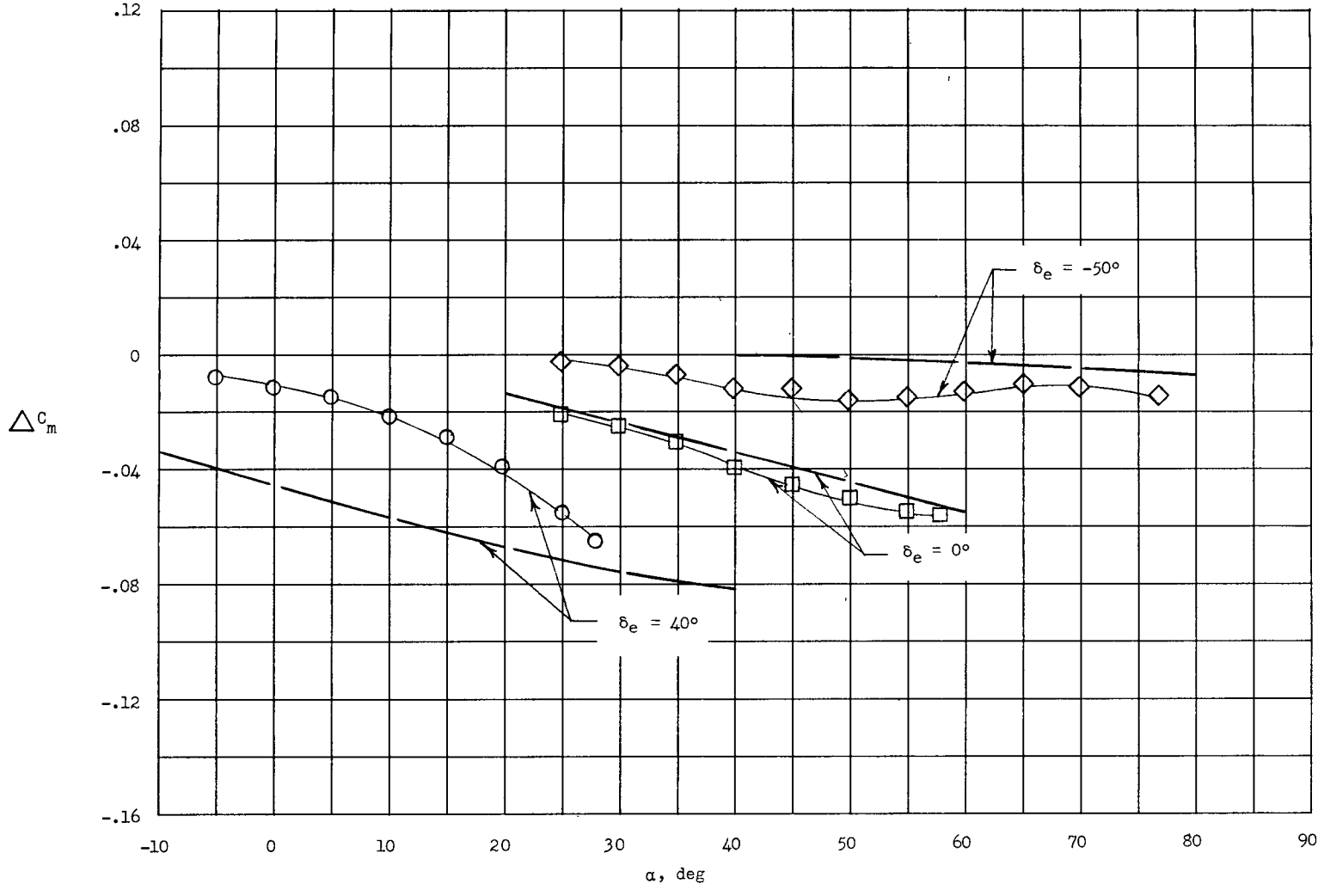

Figure 8.- Comparison of the predicted and experimental flap effectiveness of the L-1 configuration. Dashed lines indicate Newtonian theory.

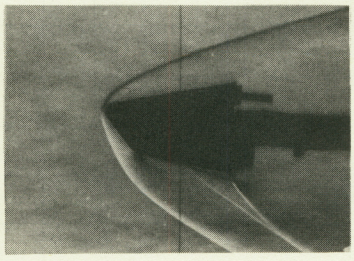

α = 5°

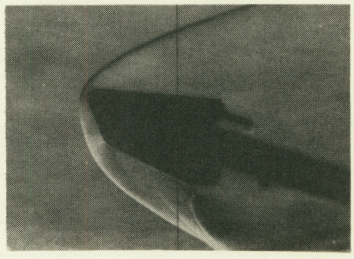

α = 20°

δ_e = 40°

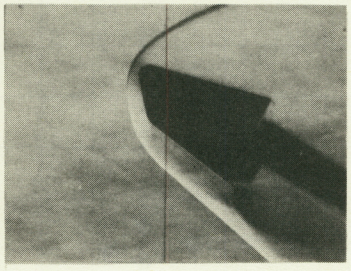

α = 30°

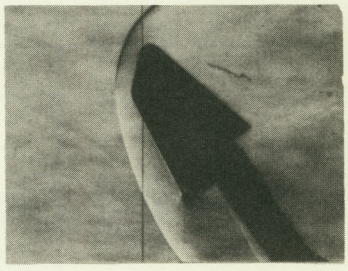

α = 55°

δ_e = 0°

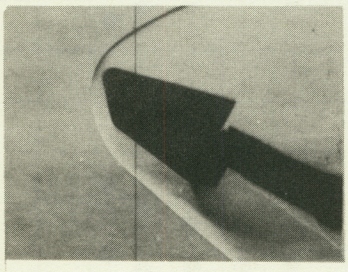

α= 30°

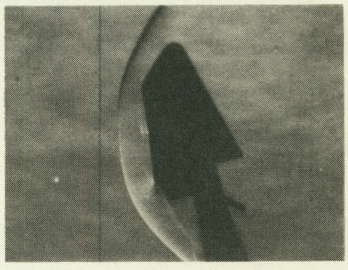

α = 75°

δ_e = -50°

L-61-8052

Figure 9.- Schlieren photographs of L-1 configuration for various flap deflections.

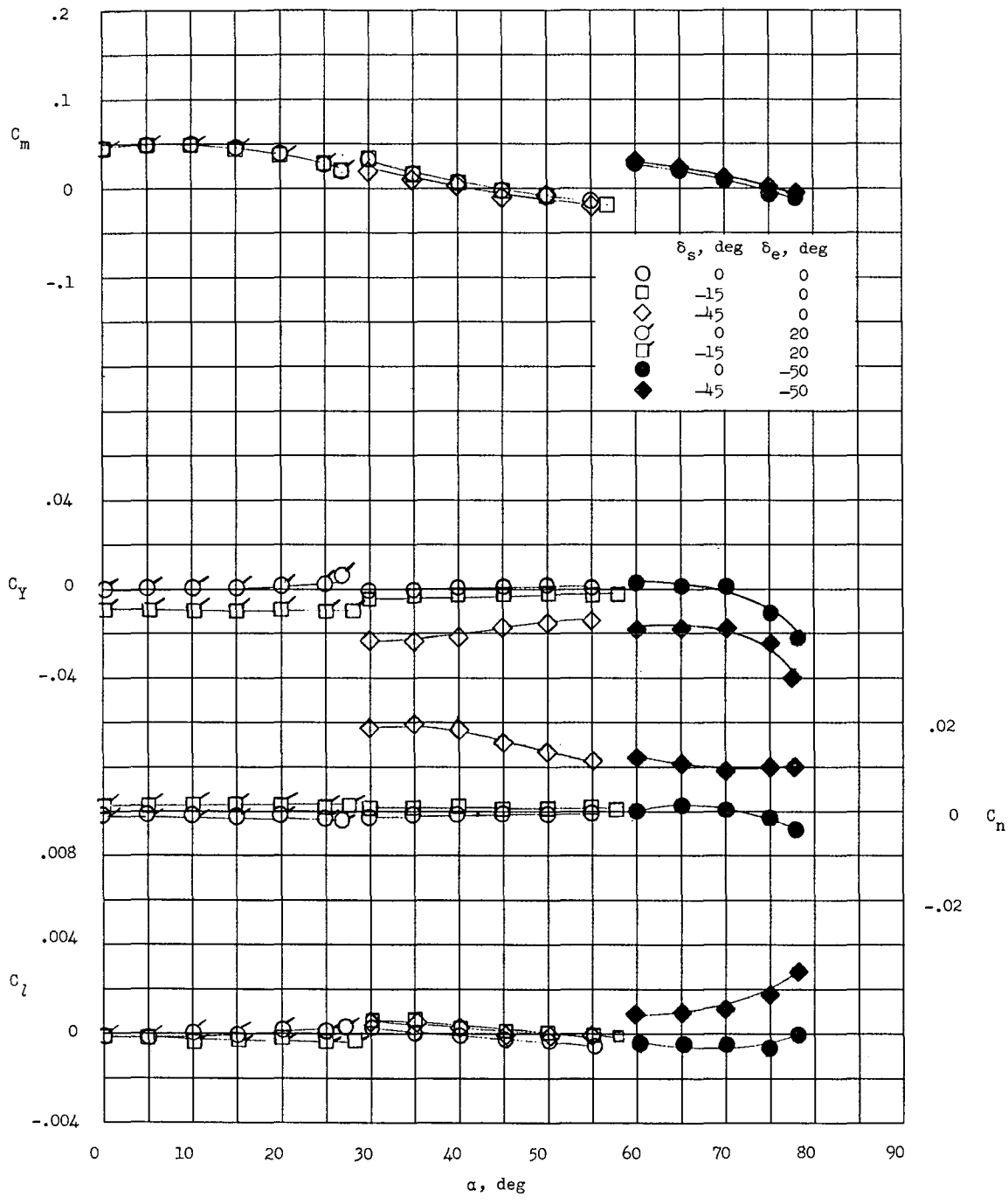

Figure 10.- Experimental yaw control characteristics of the L-1 configuration.

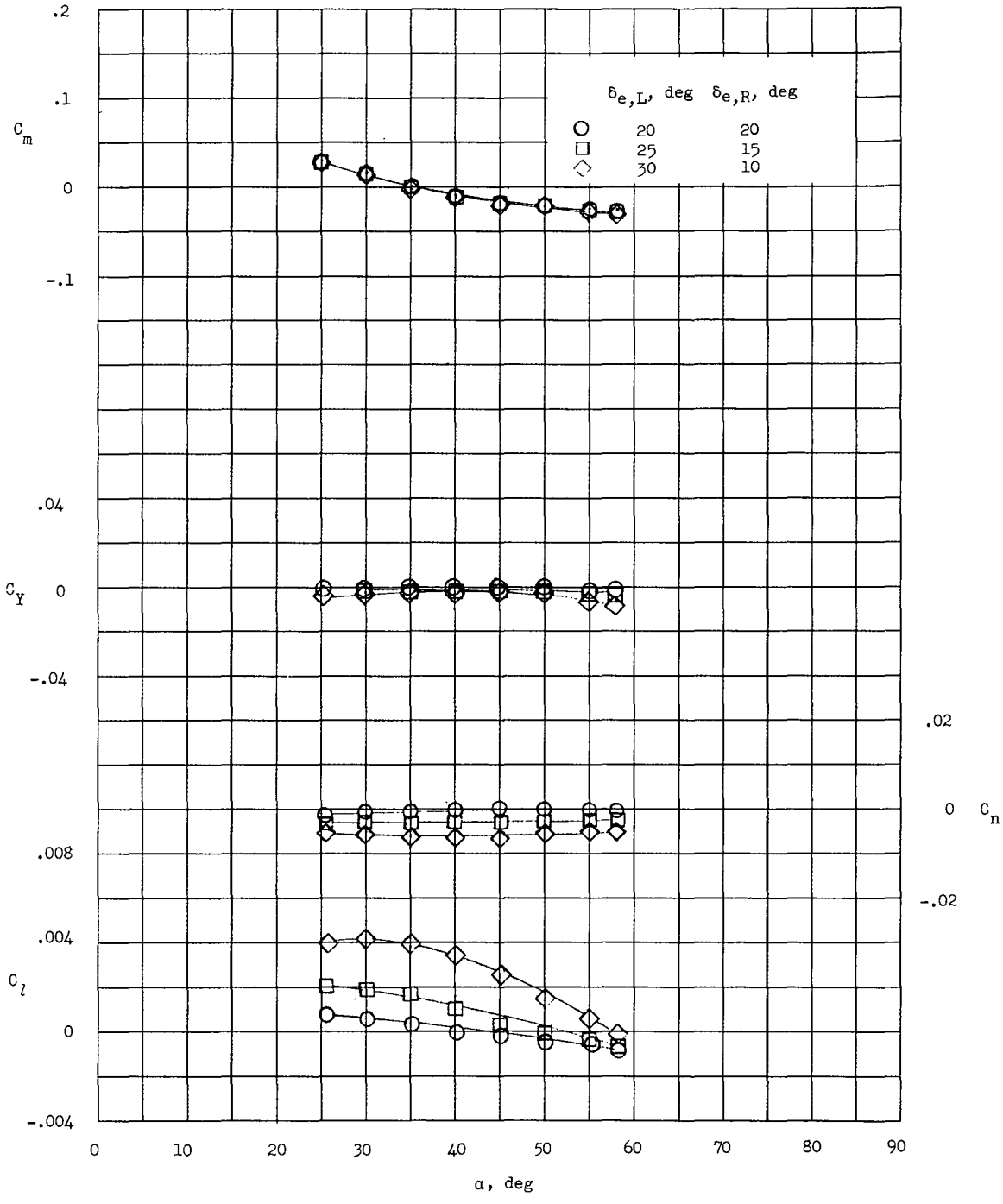

Figure 11.- Experimental roll control characteristics of the L-1 configuration. $\delta_s = 0^o$.

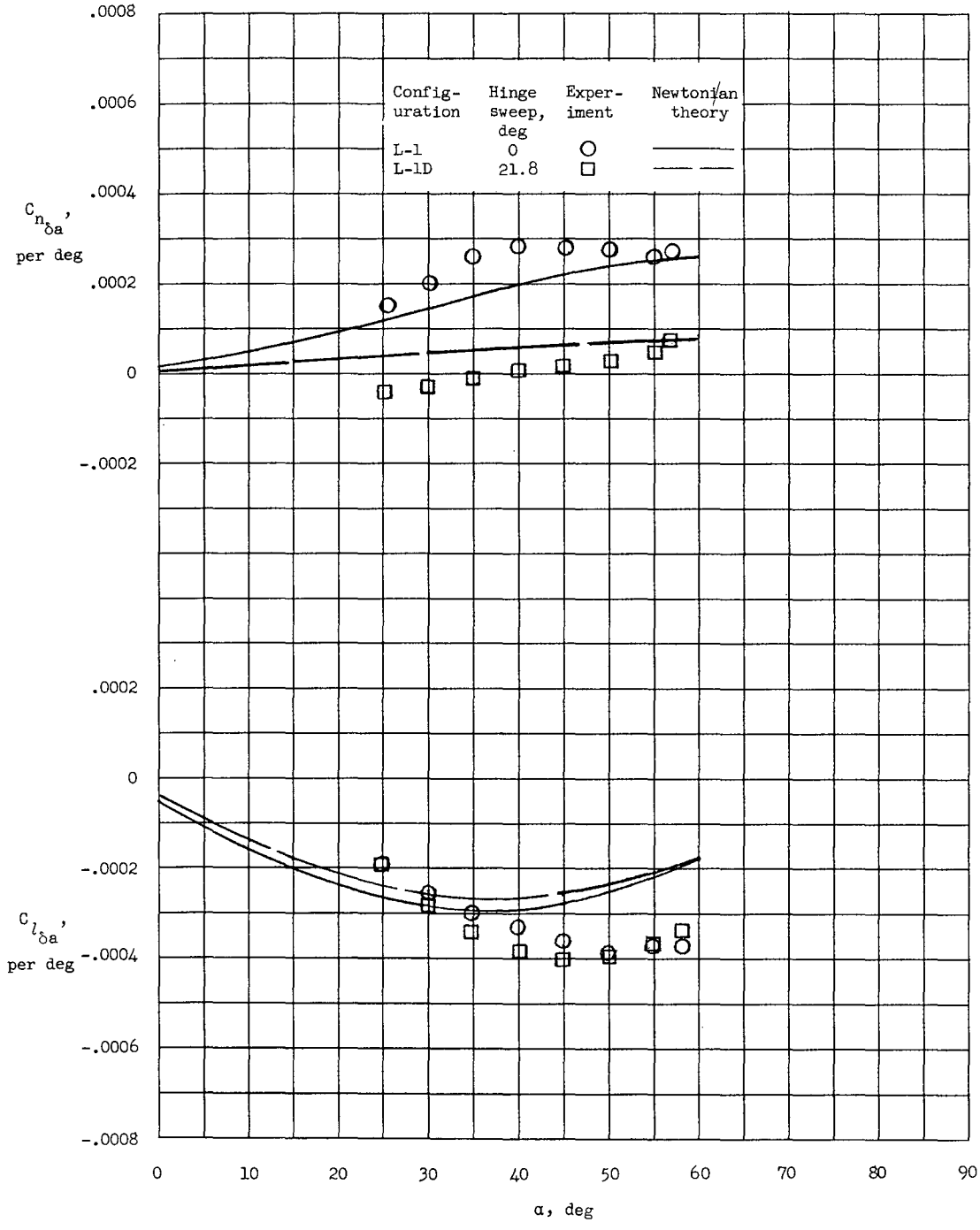

Figure 12.- Effect of hinge sweep on the roll and yaw characteristics of the configurations with differentially deflected horizontal flap. $\delta_e = 20^\circ$.

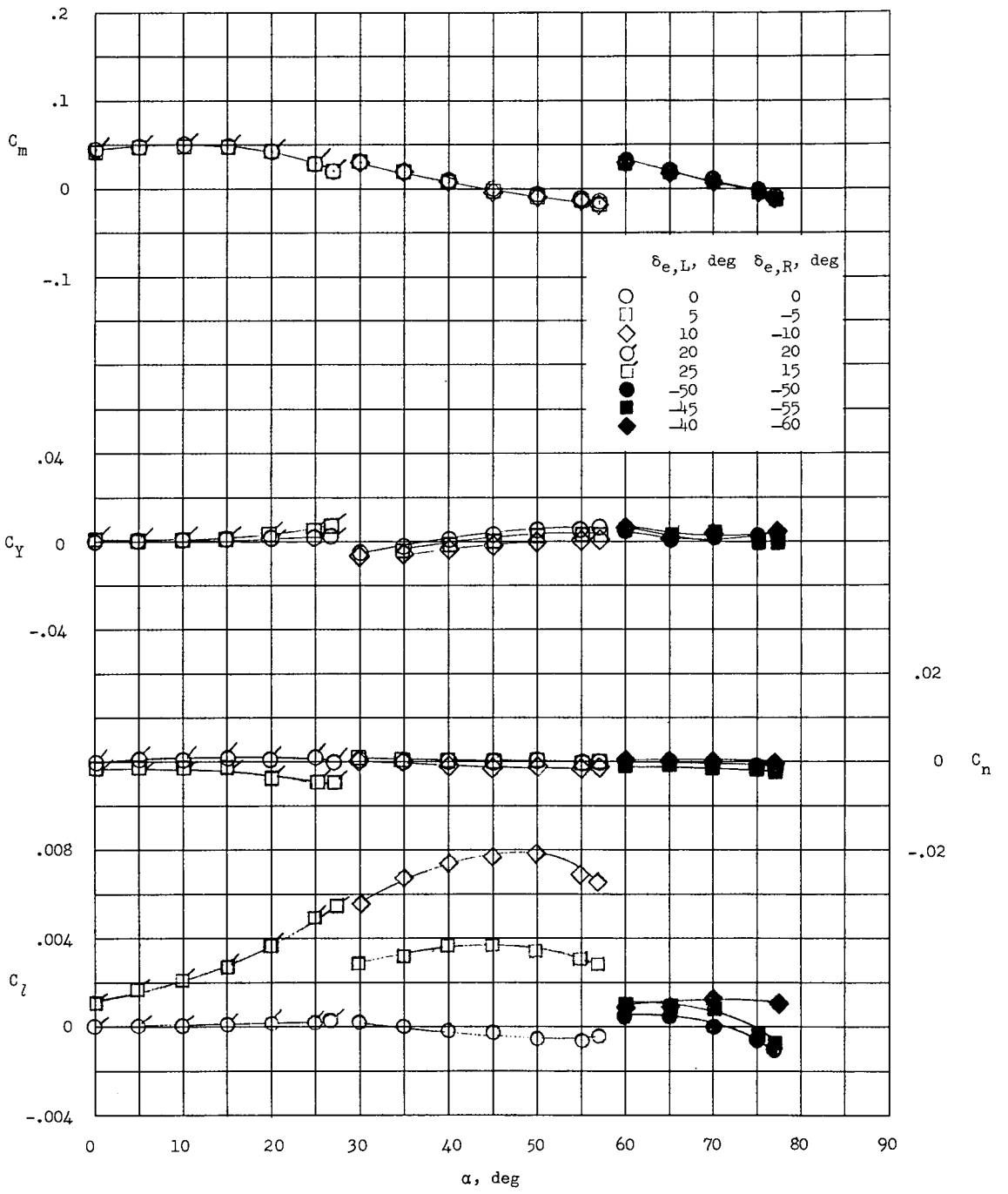

Figure 13.- Experimental roll control characteristics of the L-1D configuration. $\delta_s = 0^o$.

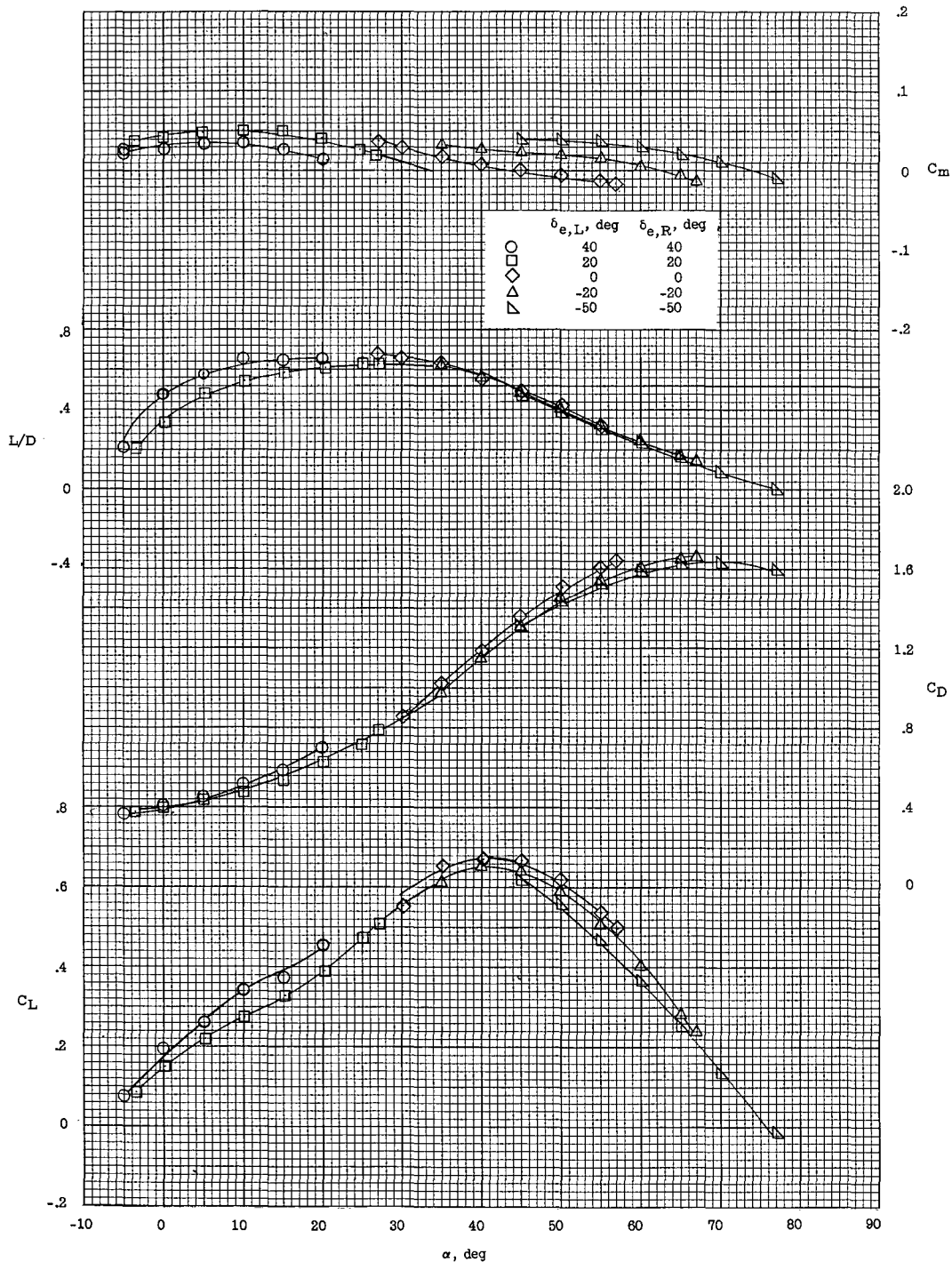

Figure 14.- Experimental trimmed longitudinal aerodynamic characteristics of the L-1D configuration. $\delta_s = 0^o$.

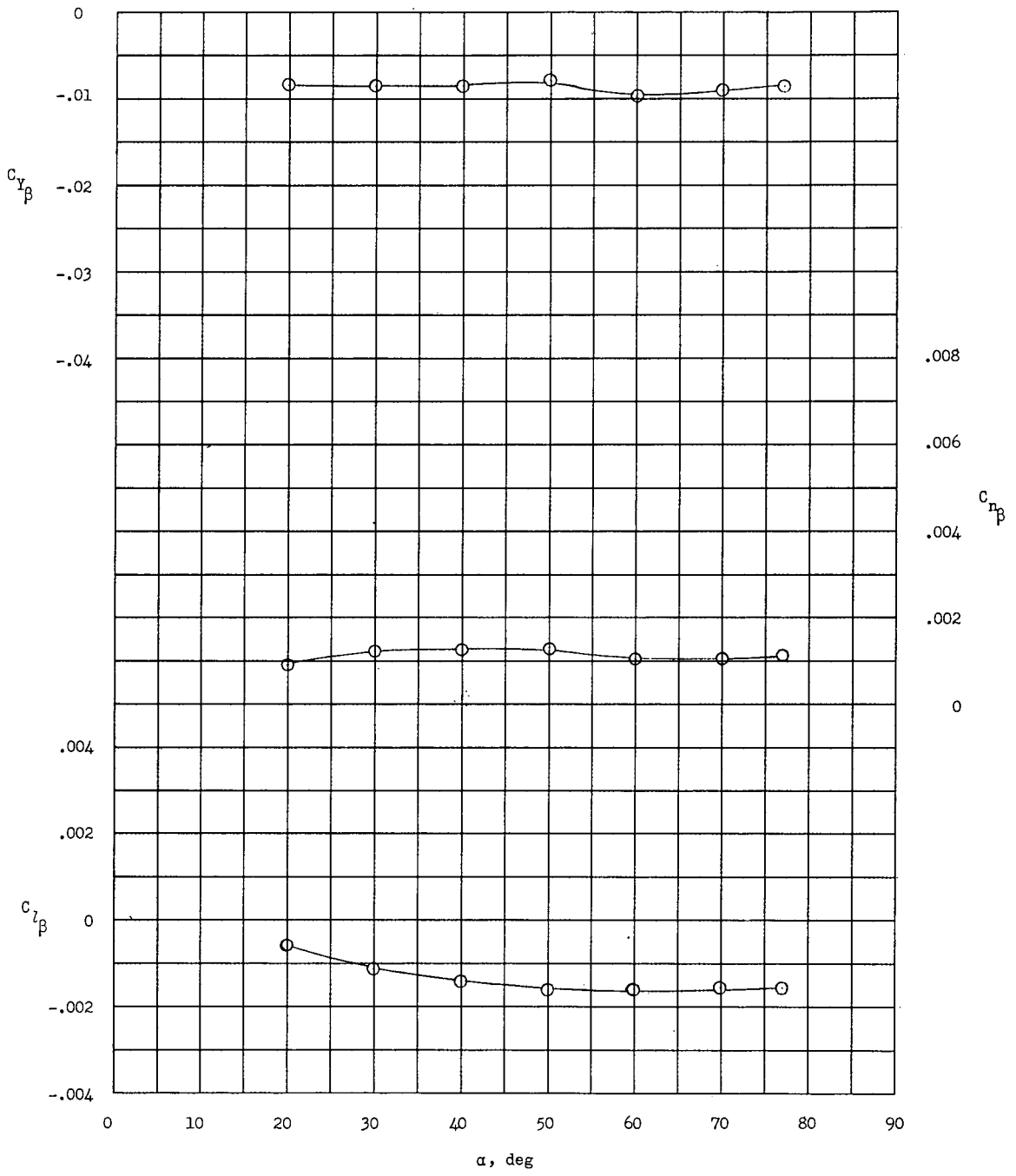

Figure 15.- Experimental longitudinally trimmed lateral stability characteristics of the L-1D configuration.

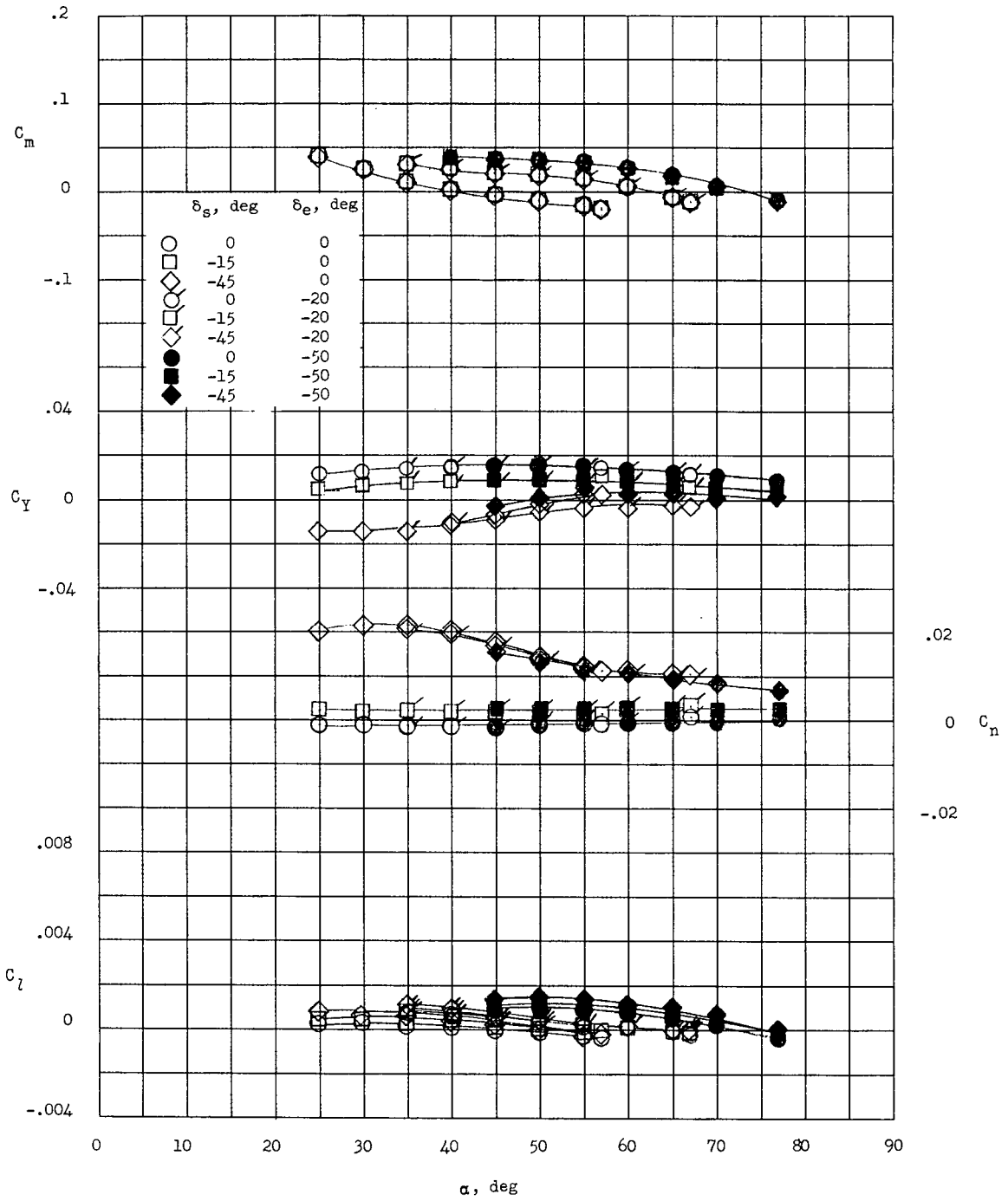

Figure 16.- Experimental yaw control characteristics of the L-1D configuration.

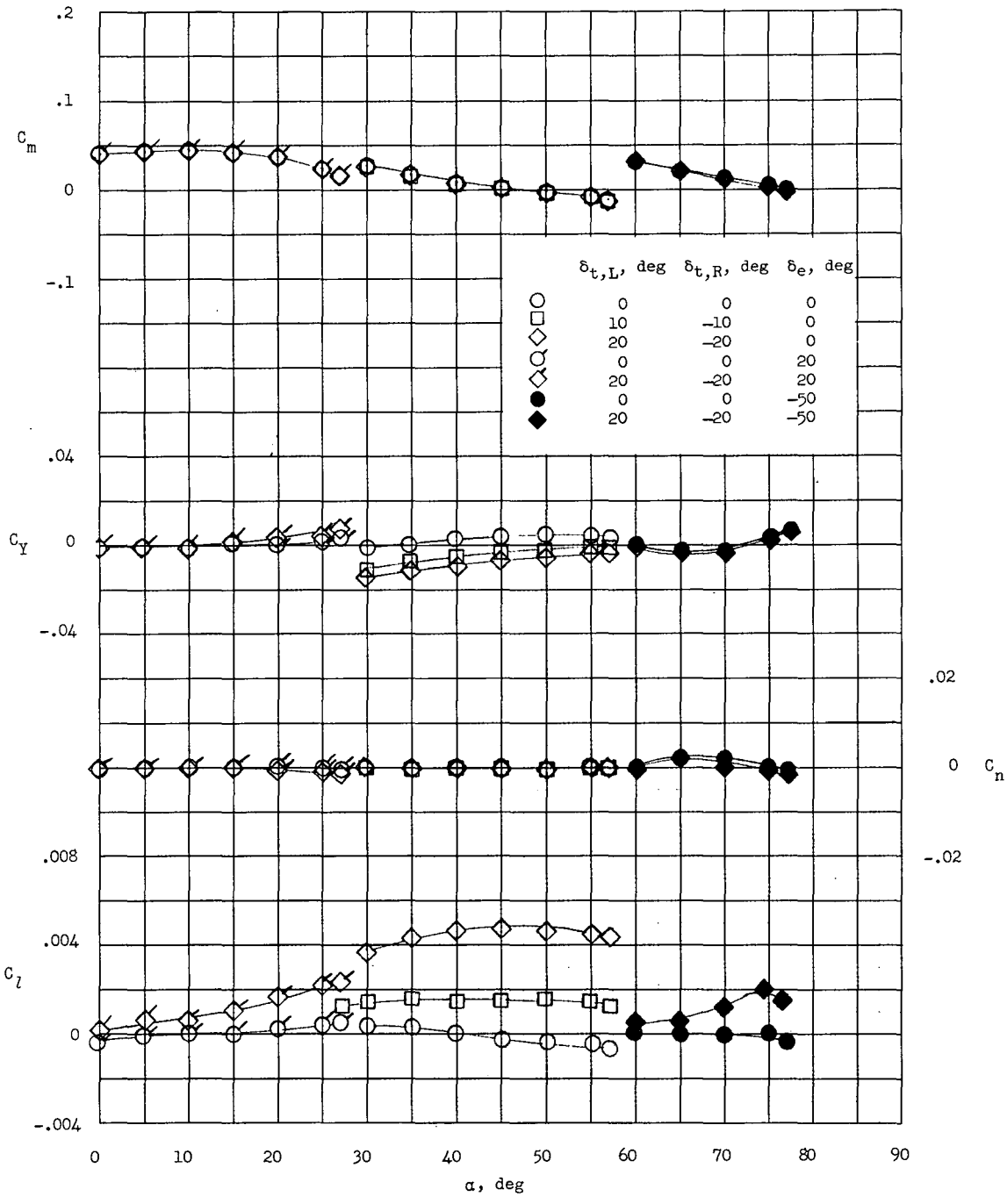

Figure 17.- Experimental roll control characteristics of the L-1B configuration. $\delta_s = 0^o$.

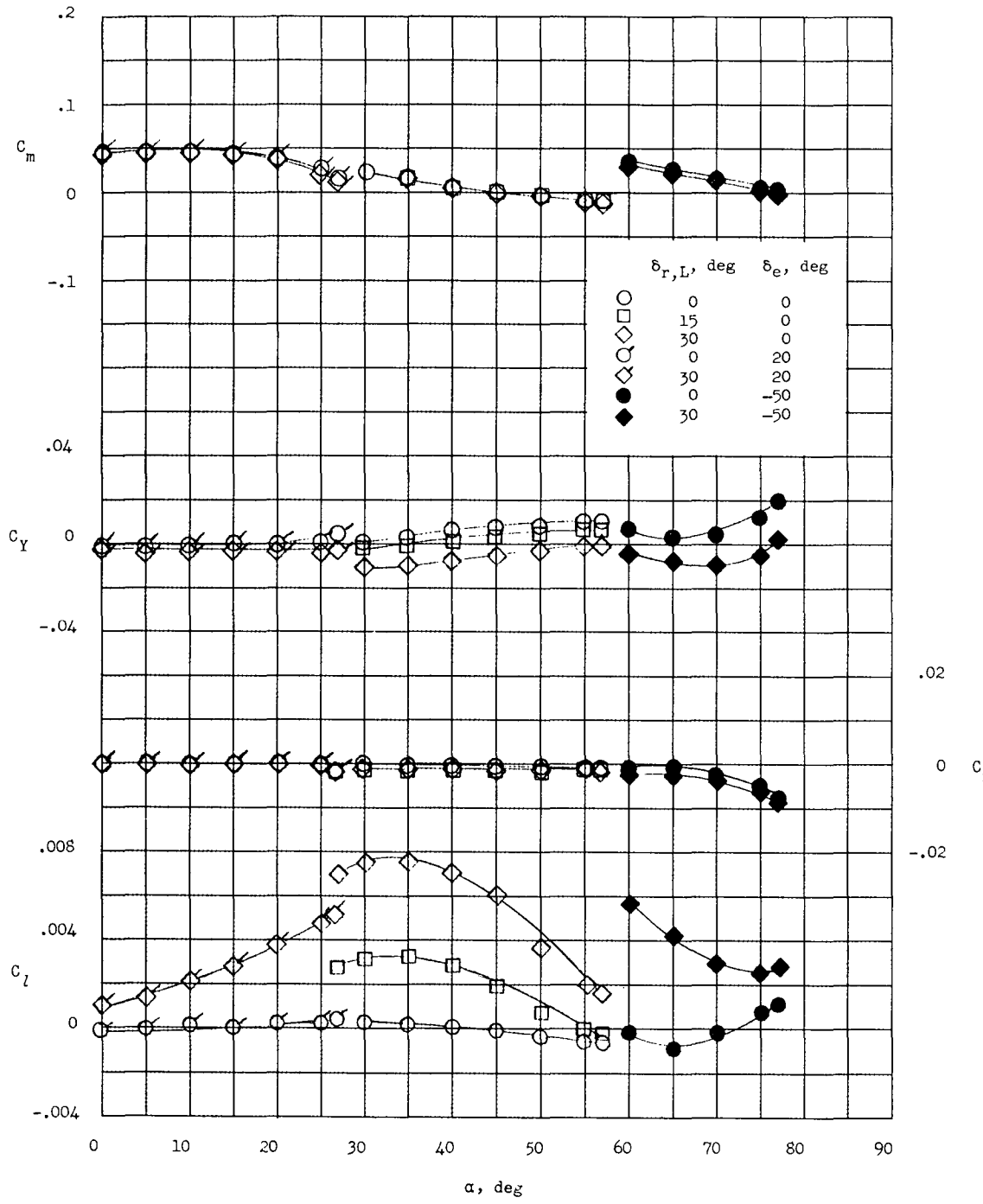

Figure 18.- Experimental roll control characteristics of the L-1C configuration. $\delta_s = 0^\circ$.

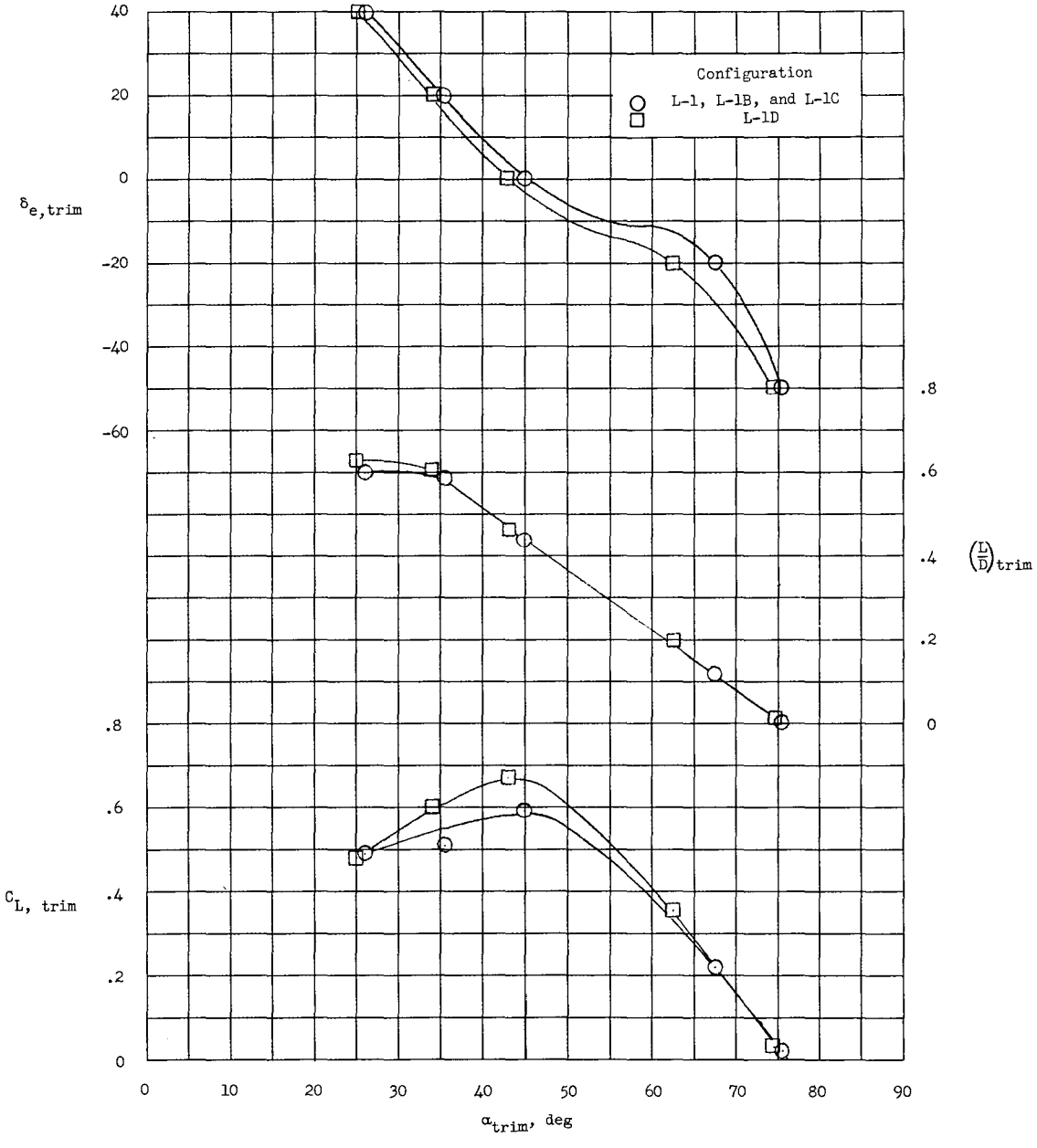

Figure 19.- Trim characteristics of L-1 series configurations.